Texture analysis of hippocampus for epilepsy

Kourosh Jafari-Khouzani,[*a,b] Mohammad-Reza Siadat,[a,b] Hamid Soltanian-Zadeh,[b,c] Kost Elisevich[d]

[a]Computer Science Department, Wayne State University, Detroit, MI 48202, USA
[b]Radiology Image Analysis Lab., Henry Ford Health System, Detroit, MI 48202, USA
[c]Electrical and Computer Engineering Dept., University of Tehran, Tehran 14395, Iran
[d]Neurosurgery Dept., Henry Ford Health System, Detroit, MI 48202, USA

ABSTRACT

This paper presents our recent study to evaluate how effectively the image texture information within the hippocampus structure can help the physicians to determine the candidates for epilepsy surgery. First we segment the hippocampus from T1-weighted images using our newly developed knowledge-based segmentation method. To extract the texture features we use multiwavelet, wavelet, and wavelet packet transforms. We calculate the energy and entropy features on each sub-band obtained by the wavelet decomposition. These texture features can be used by themselves or along with other features such as shape and average intensity to classify the hippocampi. The features are calculated on the T1-weighted and FLAIR MR images. Using these features, a clustering algorithm is applied to classify each hippocampus. To find the optimal basis, we use several different bases for wavelet and multiwavelet transforms, and compare the final classification performances, which is evaluated by correct classification rate (CCR). We use MRI of 14 epileptic patients along with their EEG results in our study. We use the pre-operative MR images of the patients who have already been determined as candidates for an epilepsy surgery using the gold standard (more costly and painful) methods of EEG phase II study. Experimental results show that the texture features may predict the candidacy for epilepsy surgery. If successful in large population studies, the proposed non-invasive method can replace invasive and costly EEG studies.

Keywords: Epilepsy, medical image processing, image segmentation, texture analysis, wavelet transform

1. INTRODUCTION

One in every 200 people within the United States (US) suffers from a neurological disease referred to as “epilepsy.” Two-thirds of all epileptic patients have a specific focal area of seizure onset within the brain. More than 20% of the epileptic patients undergo surgery when treatment with medication is ineffective, i.e., nearly 250,000 patients are potential candidates for epileptic surgery in the US. The conventional gold standard method of evaluating an epileptic patient for surgical candidacy is lengthy, painful, and costly. It requires EEG exams to detect irritative zones. A phase I EEG exam requires admittance to the hospital for a period of five to seven days. During this hospital stay, the patient undergoes 24 hour video monitoring and EEG recording and analysis (with electrodes placed at several sites on the head). If the epileptic foci is not sufficiently localized in phase I, the patient will need to undergo phase II of the surgical evaluation which involves implantation of electrodes intracranially and monitoring the patient for nearly two weeks. The current cost of the pre-surgical evaluation ranges from a few thousand dollars (screening phase) to upwards of $50,000 (an involved phase II).

Recently, it has been shown that the determination of structural and volumetric asymmetries in the human brain from MRI provides critical data for the diagnosis of focal abnormality. This has been the case with complex partial seizures attributable to hippocampal sclerosis and has been further applied to other brain regions for the same purpose. The hippocampus is an important component of the human brain's limbic system. It is strongly believed that this structure has a key role in learning process and memory. The variations in volume and architecture of the hippocampus have been observed with some brain diseases such as schizophrenia, epilepsy, and Alzheimer.[1,2]

[*] Correspondences to: ak4822@wayne.edu, msiadat@cs.wayne.edu, hamids@rad.hfh.edu. URL: http://radiologyresearch.org

Medical Imaging 2003: Physiology and Function: Methods, Systems, and Applications, Anne V. Clough, Amir A. Amini, Editors, Proceedings of SPIE Vol. 5031 (2003) © 2003 SPIE · 1605-7422/03/$15.00

Current methods for identification, segmentation and analysis of specific brain structures from MRI (manual segmentation by an expert) are labor-intensive, costly, require an expert operator, and are not reproducible. On the other hand the existing quantitative MRI analysis methods merely consider the volume of the structure of interest, e.g., the hippocampus. This is inspired by the fact that the most common site of origin in focal epilepsy is the medial temporal lobe, which contains the hippocampal formation. The mechanism of a seizure involves a cascade of neurons from a central focus. Over time this causes excitotoxic injury in the epileptic focus.

Recently, the application of hippocampal volumetry has become an accepted way to distinguish unilateral atrophy. However, some patients in whom EEG study has failed to unequivocally identify a unilateral onset have demonstrated total hippocampal volumes that do not differ unilaterally. On the other hand, in chronic partial epilepsy, there is a progressive loss of neurons secondary to excitotoxic injury. This causes a reduction of gray matter partial volume (signal) over that of white matter partial volume (signal) in the hippocampus. Therefore, the MRI signal in the hippocampus will change from the normal state.

In addition to volumetry, we analyze the MRI signal (image gray levels) in each hippocampus to get a more sensitive and specific means for determining the site of partial epilepsy of mesial temporal origin. We use the 3D T1-weighted images of the brain to segment the hippocampus structure, and the 3D FLAIR images to get textural information of each hippocampus. We examine different tools of texture analysis including multiwavelet, scalar wavelet, and wavelet packet transforms. After calculating the vector of features for a set of patients, we use fuzzy c-means clustering algorithm to classify them into two groups of normal and abnormal. We also show scatter plots of features that discriminate between the left and right abnormal hippocampi. The methods developed in this project are evaluated by the current gold standard of EEG phase II studies.

The outline of this paper is as follows. In Section 2 we describe the method we used to segment the hippocampus from MR images of the brain. In Section 3 we review some texture analysis methods used in this research. In Section 4 we propose a classification method to classify each hippocampus to normal and abnormal, and finally in Section 5 we present the experimental results.

2. HIPPOCAMPUS SEGMENTATION

The first step is to segment the hippocampus from the 3D MR images of the brain. To reach this goal we use T1-weighted images as they show structure of hippocampus better than FLAIR images. The hippocampus is characterized by multiple edges and missing boundaries. As a result, segmentation of this structure is extremely challenging. The proposed segmentation method has two steps and is fully automatic. The first step is hippocampus localization and the second step utilizes a 3D deformable model to achieve an accurate and high-resolution segmentation.

2.1 Hippocampus localization

The localization procedure finds several landmarks around the hippocampus. We create binary images representing gray matter (GM) and cerebrospinal fluid (CSF). Using the binary images, the proposed method finds certain landmarks from specified points of view and within specified fields of search. Morphological routines are utilized to extract the connected components/segments of the landmarks. A rule-based system with a set of 35 rules is used to analyze the extracted landmarks and segments. This knowledge-based system assigns each individual landmark an intermediate confidence factor (ICNF). The ICNF shows how accurately each individual landmark/segment is found. An approximate reasoning procedure calculates an overall confidence factor (CNF) from the ICNFs. Setting a threshold for the CNF, we determine whether the hippocampus exists in a particular slice and how accurately its landmarks are found (See references[3, 4] for details). Figs. 1(a)-(b) show the results of hippocampus localization on the coronal and sagittal views of a T1-weighted MRI scan.

2.2 3D deformable model

The proposed 3D deformable model converts the localization results (as an initial polygon) to an accurate and high-resolution 3D model of the structure. The task is done by adding more vertices to the initial model and moving them iteratively based on the internal and external forces until the termination condition is met. The internal forces are calculated from local model curvature, using a least-squares error approximation method. The external forces are

calculated by applying a step expansion and restoration filter (SEF) to the image data. A solution for self-cutting problem has been proposed via principal axis analysis and re-slicing (see reference[5] for details). Two orthogonal views (coronal and sagittal) of the final result are illustrated in Figs. 1(c)-(d). A coronal FLAIR image with ROIs from the corresponding T1-weighted image is shown in Fig. 2.

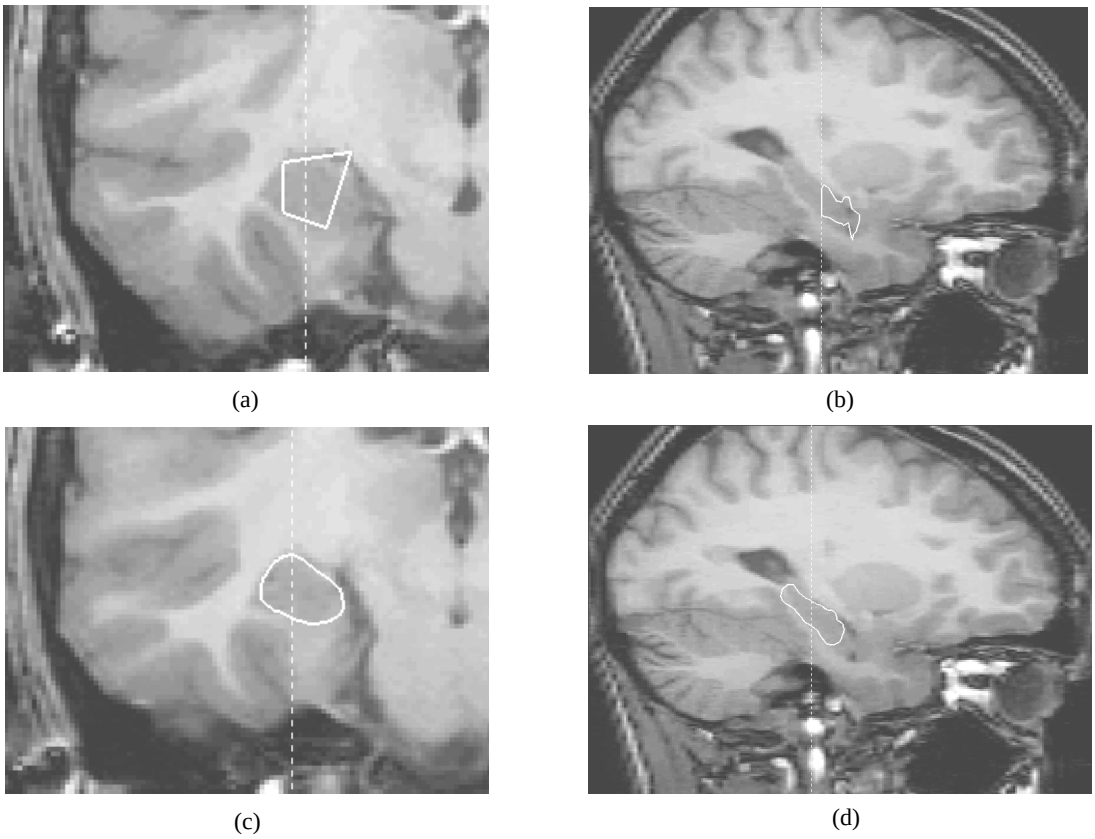

Figure 1: a, b) Hippocampal localization results on coronal and sagittal views, using the knowledge-based localization method. c, d) The segmentation results on coronal and sagittal views using the 3D deformable model.

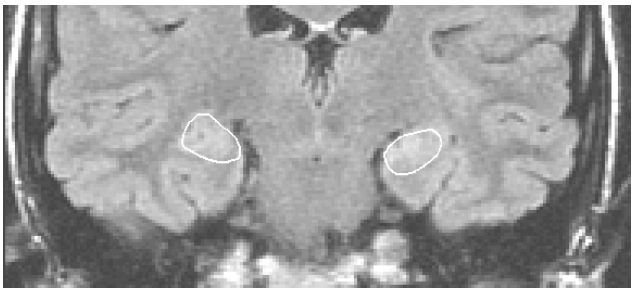

Figure 2: A Coronal FLAIR image with Hippocampus ROIs found on the corresponding T1-weighted image overlaid.

3. FEATURE EXTRACTION

Wavelet transforms are popular in texture analysis because of providing a multiresolution representation. Multiwavelet is a new concept in the framework of wavelet transform, and has some advantages compared to wavelet transform and has been successful in texture analysis of prostate pathological images.[6] In the next section, we review the multiwavelet transform.

3.1 Multiwavelet transform

While in scalar wavelet transform there is only one scaling function, in multiwavelet transform there exists more than one scaling function. Multiwavelets have important advantages compared to scalar ones. For example, features such as short support, orthogonality, symmetry and vanishing moments are known to be important in signal and image processing. A scalar wavelet cannot possess all of these properties at the same time. On the other hand, a multiwavelet system can simultaneously provide perfect reconstruction while preserving length (orthogonality), good performance at the boundaries (via linear-phase symmetry), and a high order of approximation (via vanishing moments). This suggests that multiwavelets may perform better in various applications.[7]

In multiwavelet analysis the multiscaling function $\boldsymbol{\Phi}(t)=[\phi_1(t),...,\phi_r(t)]^{\mathrm{T}}$ satisfies a two-scale dilation equation:

$$\boldsymbol{\Phi}(t)=\sqrt{2}\sum_k H_k\boldsymbol{\Phi}(2t-k) \tag{1}$$

where H_k is an $r\times r$ matrix of lowpass filter coefficients and r is called multiplicity. Like scalar wavelet function, multiwavelet function $\boldsymbol{\Psi}(t)=[\psi_1(t),...,\psi_r(t)]^T$ must satisfy the two-scale wavelet equation:

$$\boldsymbol{\Psi}(t)=\sqrt{2}\sum_k G_k\boldsymbol{\Phi}(2t-k) \tag{2}$$

where G_k is an $r\times r$ matrix of highpass filter coefficients.

Assume $V_j=\overline{\mathrm{span}\left\{2^{j/2}\phi_i\left(2^j t-k\right),1\le i\le r,k\in \mathrm{Z}\right\}}$, then if $f(t)$ is in V_0, it can be expanded by a linear combination of multiscaling and multiwavelet functions:

$$f(t)=\sum_k \boldsymbol{c}_{J_0,k}{}^T\boldsymbol{\Phi}_{J_0,k}(t)+\sum_{j=J_0}^{\infty}\sum_k \boldsymbol{d}_{j,k}{}^T\boldsymbol{\Psi}_{j,k}(t) \tag{3}$$

where $\boldsymbol{c}_{j,k}=\left[c_{1,j,k},...,c_{r,j,k}\right]^T$ and $\boldsymbol{d}_{j,k}=\left[d_{1,j,k},...,d_{r,j,k}\right]^T$ are coefficients of the multiscaling and multiwavelet functions respectively, and $\boldsymbol{\Phi}_{j,k}(t)=2^{j/2}\boldsymbol{\Phi}\left(2^j t-k\right)$, $\boldsymbol{\Psi}_{j,k}(t)=2^{j/2}\boldsymbol{\Psi}\left(2^j t-k\right)$. Based on (1) and (2) we can conclude:

$$\boldsymbol{c}_{j-1,k}=\sum_n H_n\boldsymbol{c}_{j,2k+n} \tag{4}$$

$$\boldsymbol{d}_{j-1,k}=\sum_n G_n\boldsymbol{d}_{j,2k+n} \tag{5}$$

In this research we use multiwavelets with multiplicity r = 2. The ralations (4) and (5) can be illustrated by multiwavelet filterbank shown in Fig. 3. The lowpass filter and highpass filter consist of coefficients corresponding to the dilation equation (1) and wavelet equation (2) and these coefficients are matrices, so during the convolution step they must multiply vectors (instead of scalars). This means that multifilter banks need input rows. Thus, a method for vectorization of scalar input should be used. This is called preprocessing and different approaches to preprocessing have been developed.[8, 9] In this research, we use the familiar repeated row and critically sampled approaches.

In repeated row approach the input signal is repeated to get an input vector.[7] This introduces oversampling of the data by a factor of two. There is also an alternative version of repeated row preprocessing in which the first row of input vector is the signal and the second row is the signal multiplied by α:

$$\boldsymbol{c}_{0,k} = \begin{bmatrix} c_{1,0,k} \\ c_{2,0,k} \end{bmatrix} = \begin{bmatrix} f[k] \\ \alpha f[k] \end{bmatrix} \tag{6}$$

The parameter α is chosen such that if the input signal is constant, the output of the high-pass multifilter is zero.[10] We use this kind of repeated row preprocessing.

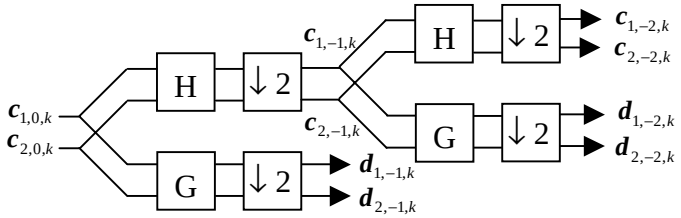

Figure 3: Multiwavelet filterbank, showing 2 levels of decomposition.

In critically sampled approach the input signal is preprocessed such that a critically sampled representation is maintained. If the data enters at rate *R*, preprocessing yields two streams at rate *R*/2 for input to the multifilter. We used a critically sampled preprocessing based on the approximation properties of the continuous multiwavelets.[7] The symmetric extension of signal has also been used as described in reference[7] to preserve critically sampling nature of system in filtering the signals at their boundaries. This approach can be used for symmetric or antisymmetric filter banks. All the multiwavelets that we used in this research have symmetric or antisymmetric filter banks.

3.2 Multiwavelet transform of images

For calculating multiwavelet transform of images, we can use tensor product method, i.e., performing the 1-D algorithm in each dimension separately.[7] Fig. 4 shows the submatrices resulting from one and two levels of 2-D multiwavelet decomposition. The result after first decomposition can be represented as the following matrix:

$$\begin{array}{cccc} L_1L_1 & L_2L_1 & H_1L_1 & H_2L_1 \\ L_1L_2 & L_2L_2 & H_1L_2 & H_2L_2 \\ L_1H_1 & L_2H_1 & H_1H_1 & H_2H_1 \\ L_1H_2 & L_2H_2 & H_1H_2 & H_2H_2 \end{array}$$

where each entry represents a subband, corresponding to lowpass and highpass filters used in vertical and horizontal directions. For example, the subband labeled L_1H_2 corresponds to data obtained by applying the highpass filter on the horizontal direction and taking its second channel, then applying lowpass filter on the vertical direction and taking its first channel (refer to Fig. 3). The next level of decomposition will decompose the following "low-low pass" submatrix, in a similar manner:

$$\begin{array}{cc} L_1L_1 & L_2L_1 \\ L_1L_2 & L_2L_2 \end{array}$$

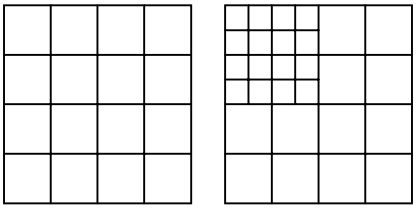

(a) (b)

Figure 4: Result of 2-D multiwavelet decomposition. (a) One level of decomposition. (b) Two levels of decomposition.

3.3 Multiwavelet features

The energy and entropy of the multiwavelet coefficients are calculated as features for classification. As indicated in Fig. 4, the result of decomposition is a number of submatrices. From each submatrix $[x_{ij}]$, the following features are calculated:

$$Energy = \frac{\sum_i \sum_j {x_{ij}}^2}{N \times N} \tag{7}$$

$$Entropy = \frac{-1}{\log N^2} \sum_i \sum_j \left[\frac{{x_{ij}}^2}{norm^2} \right] \log \left[\frac{{x_{ij}}^2}{norm^2} \right] \tag{8}$$

where $norm^2 = \sum_i \sum_j {x_{ij}}^2$ and N is the dimension of each submatrix; its use in the above equation permits features remain in particular ranges regardless of submatrices dimensions. Energy shows the amount of signal in a specific resolution, while entropy shows the non-uniformity of the submatrices values. In this work, we use 3 different multiwavelets: GHM,[11] CL,[12] and SA4.[13]

3.4 Scalar wavelet and wavelet packet features

Scalar wavelet and wavelet packets have also been successful in texture analysis.[14, 15] To compare different methods of feature extraction for the hippocampus, we use scalar wavelet as well as wavelet packet transform, which extends filter banks to high resolutions. We first decompose each image to submatrices and then compute the same features as those of the multiwavelet decomposition given in (7) and (8). We use D_6 and D_{20} bases,[14] since these two wavelets generated superior results compared to other well-known wavelets.

3.5 Computing the features for hippocampus

One difficulty with the feature extraction using wavelet transform is that we need a rectangular image to compute the wavelet transform, while hippocampus does not have this characteristic. To solve this problem, after segmentation we inscribe the hippocampus in a rectangular prism. Then we analyze each coronal slice of this volume separately. In each slice, there is always an empty space, which should be filled (see Fig. 5). If we set the intensity values of the empty part equal to zero, the sharp edges will significantly affect the outcome of wavelet transform, the extracted features and the classification results. One method to overcome this problem is to set the empty part equal to the average intensity. However this method also adds some extra edges, which affect the results. The other method is to dilate the image repeatedly with a 3×3 window and filling the dilated part by the average of its 8-connected neighbors, which fall in the non-empty part of the image. For each slice we inscribe the non-empty part of the hippocampus in a square and fill the empty space of this square with the above method. This is depicted in Figs. 5 and 6.

An important practical issue in extracting intensity-based features is that, FLAIR images of different patients have different ranges of intensities, which may considerably affect the energy of different frequency bands of the wavelet transform. In order to reduce this effect, before computing the wavelet transform, we may divide the gray level values of each hippocampus by its mean or standard deviation. But, this method removes the relative intensity information of the right and left hippocampi, which may be an important feature; an abnormal hippocampus is expected to have a lower volume and a higher FALIR intensity. An alternative method to normalize, while preserving the relative intensity information, is to divide the intensities of each hippocampus by the average intensity of the other hippocampus (i.e. right

by left and vice versa). In this case, for each patient the average of intensity ratios will become less than one for the normal hippocampus, and more than one for the abnormal hippocampus (the abnormal one is the brighter one). After computing the wavelet transform of each slice and calculating the predefined features for each slice, we average the features over all slices. As it is often the case, only one of the hippocampi has problem in each patient. To get one set of features for each patient we divide the resulting features of the right hippocampus (i.e. energy, entropy, and volume) by the resulting features of the left hippocampus and use these ratios as the final set of features for each patient.

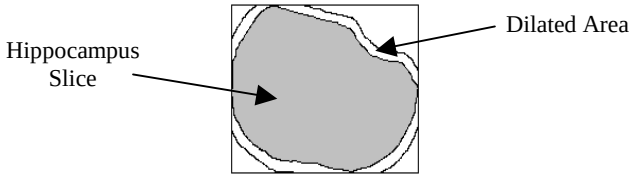

Figure 5: Filling the empty area by repeated dilations and avearaging.

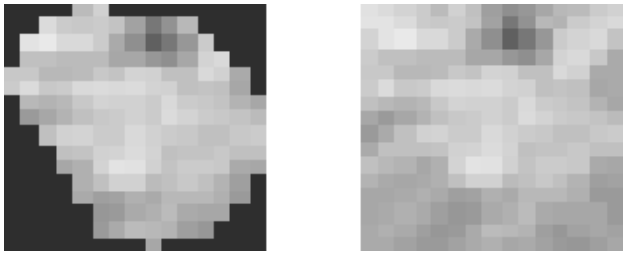

Figure 6: Segmented hippocampus image, a) before filling the empty area, b) after filling the empty area.

4. CLASSIFICATION

After computing different kinds of features explained in Section 3 for each patient, we classify them into two classes using fuzzy c-means algorithm.[16] To determine how effectively the normal and abnormal hippocampi are separated, we use the EEG phase II results as the gold standard and compute the correct classification percentage by counting the misclassified hippocampi.

5. EXPERIMENTAL RESULTS

Table 1 shows the correct classification percentages using different combination of features. In this table R.R. and C.S. stand for repeated row and critically sampled preprocessing respectively. Energy and entropy ratio features are used separately as well as together for classification. For scalar wavelet transform we used D_6 and D_{20} bases with one and two levels of decomposition. For multiwavelet transform we used GHM, CL, and SA4 bases using repeated row and critically sampled preprocessing with only one level of decomposition since higher levels of decomposition need larger images while hippocampus images are relatively small. For wavelet packet we used two levels of decomposition. A combination of energy, entropy and volume ratio features is also reported. Table 2 shows the results of classification using only volume ratio (right/left) as feature. We used thresholding method to classify them. If the ratio is more than 1.00 we label the left hippocampus abnormal and if it is less than 1.00, the right hippocampus is labeled abnormal.

As we see from Table 1, the energy ratio has good classification capability while except for the multiwavelets, entropy has poor classification results. Moreover, its combination with energy features does not improve the classification. In some cases, volume ratio increases the classification accuracy but the results do not exceed 92.86%, which can also be achieved by the energy features of the D_{20} wavelet packet transform alone. This may suggest that the entropy and

volume features do not add extra information to the set of energy features. Moreover, note that wavelet bases affect the classification results. In order to get the most accurate results we should examine different wavelet bases. As shown in Table 2, using volume ratio as feature, results in 64.28% correct classification. This means volume ratio has limited classification ability.

Table 1: Correct classification percentages using different methods for feature extraction.

				Correct Classification Percentage			
Method	Type	Levels of Decomposition		Energy Ratio	Entropy Ratio	Energy & Entropy Ratios	Energy, Entropy, and volume ratios
Wavelet	D_6	1		78.57	50.00	78.57	85.71
		2		85.71	57.14	85.71	85.71
	D_{20}	1		85.71	50.00	85.71	85.71
		2		78.57	57.14	78.57	78.57
Multiwavelet	GHM	1	R.R.	78.57	85.71	78.57	78.57
			C.S.	71.43	78.57	71.43	71.43
	CL	1	R.R.	85.71	85.71	85.71	78.57
			C.S.	78.57	71.43	78.57	78.57
	SA4	1	R.R.	78.57	78.57	78.57	85.71
			C.S.	85.71	71.43	85.71	85.71
Wavelet Packet	D_6	2		85.71	50.00	85.71	85.71
	D_{20}	2		92.86	64.29	92.86	92.86

Table 2: Results of classification using thresholding and volume ratio feature. “C” and “IC” stand for correct and incorrect classification respectively.

Patient #	1	2	3	4	5	6	7	8	9	10	11	12	13	14
Abnormal Side	L	L	R	R	L	L	R	R	L	R	R	L	L	R
Volume Ratio	1.13	0.87	1.56	0.58	1.40	0.85	0.97	0.67	2.04	1.12	0.53	1.78	1.45	1.09
Thresholding Results	C	IC	IC	C	C	IC	C	C	C	IC	C	C	C	IC

Fig. 7 shows the cluster plots of different energy features of the D_{20} wavelet packet, which had the best separation. As shown in this figure, the clusters are linearly separable. While in Figs. 7.(a) and 7.(b) there is a good separation between the two clusters, in Figs. 7.(c) to 7.(f) the clusters are close to each other but still linearly separable. A linear classifier can result in a 100% correct classification while in Table 1 the maximum correct classification is 92.86%. This is because the results in Table 1 are based on using fuzzy c-means classifier. In this classifier the distances of the sample to the clusters centers are used. Thus, although the clusters are linearly separable, the fuzzy c-means algorithm does not provide perfect classification results. The preliminary results suggest that energy ratio features are less sensitive to segmentation accuracy compared to the volume ratio. This may be explained by the fact that the texture features are

more affected by the intensity distribution in a region rather than by the boundary and volume of a structure (which are sensitive to segmentation accuracy).

Overall, considering Fig. 7.(b) where there is a good separation between the two classes and the samples are far enough from the decision boundary, it can be concluded that texture information of the hippocampus can predict its abnormality. However, a large population study is needed to confirm this finding.

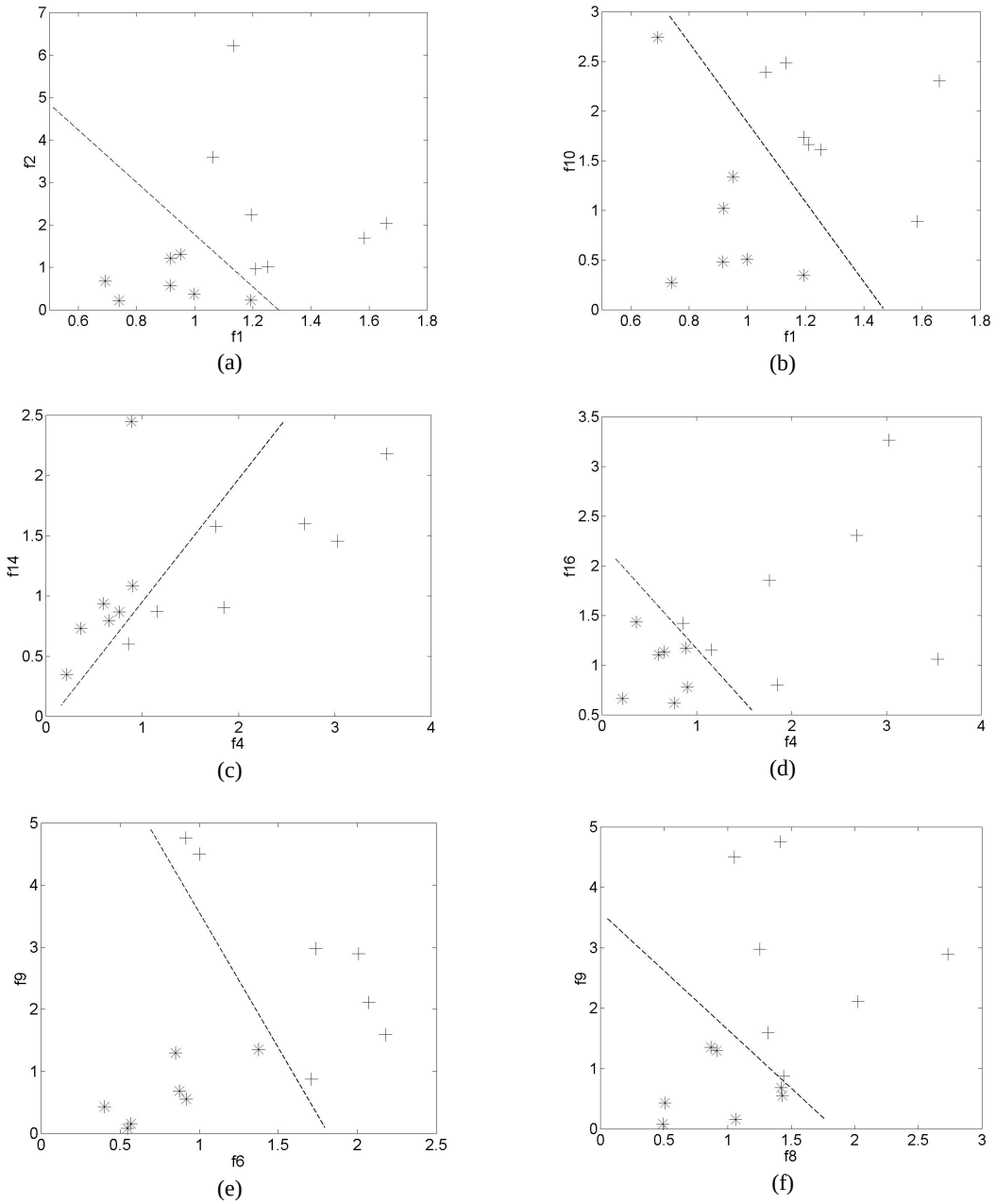

Figure 7: Cluster plots of different frequency bands using D_{20} wavelet packet. The "*" and "+" symbols respectively show the patients with left and right abnormal hippocampi (candidates for surgery on the corresponding hippocampus).

6. SUMMARY AND CONCLUSION

In this work, we used T1-weighted and FLAIR images of 14 patients. We have focused on epileptic patients with partial seizures of presumed mesial temporal origin. All patients had EEG records and most of them underwent resection of one of the hippocampi. The location of seizure onset as determined by the EEG methods and the postoperative outcomes are considered as the gold standard. Using T1-weighted images of each patient we segmented each image to get hippocampus using the method described in Section 2. Then using the methods explained in Section 3 we computed a set of features and then classified them into two groups using fuzzy c-means algorithm. For scalar wavelet transform we used D_6 and D_{20} bases with one and two levels of decomposition. For multiwavelet transform we used GHM, CL, and SA4 bases using repeated row and critically sampled preprocessing with only one level of decomposition since higher levels of decomposition need larger images while hippocampus images are relatively small. For wavelet packet we used two levels of decomposition. The results demonstrate that energy features derived from wavelet transform can predict the abnormality of the hippocampus in patients with partial seizures of presumed mesial temporal origin. Further large population studies are needed to confirm this finding.

REFERENCES

1. C.R. Jack, R.C. Petersen, P.C. O'Brien, and E.G. Tangalos: "MR-based hippocampal volumetry in the diagnosis of Alzheimer's disease," *Neurology* **42**, no. 1, pp. 183-8, 1992.
2. F. Cendes, F. Andermann, P. Gloor, A. Evans, M. Jones-Gotman, C. Watson, D. Melanson, A. Olivier, T. Peters, I. Lopes-Cendes, et al. "MRI volumetric measurement of amygdala and hippocampus in temporal lobe epilepsy," *Neurology*, **43**, no. 4, pp. 719-25, 1993.
3. M. Siadat, H. Soltanian-Zadeh, "An Intelligent Approach for Locating Hippocampus in Human Brain MRI," *Proc. 16th IASTED AI'98 Conf.*, Feb. 1998.
4. H. Soltanian-Zadeh, M. Siadat, "Knowledge-Based Localization of Hippocampus in Human Brain MRI," *SPIE* **3661**, pp. 1646-1655, 1999.
5. A. Ghanei, H. Soltanian-Zadeh, K. Elisevich, J. A. Fessler, "Knowledge-Based Deformable Surface Model with Application to Segmentation of Brain Structures in MRI," *SPIE* **4322**, pp. 356-365, 2001.
6. K. Jafari-Khouzani, H. Soltanian-Zadeh, "Multiwavelet Grading of Pathological Images of Prostate," *IEEE Trans. on Biomedical Engineering.*, in press, 2003.
7. V. Strela, P. Heller, G. Strang, P. Topiwala, and C. Heil, "The application of multiwavelet filterbanks to signal and image processing," *IEEE Trans. Image Proc.* **8**, no. 4, pp. 548-563, 1999.
8. X. G. Xia, J. S. Geronimo, D. P. Hardin, and B. W. Suter, "Design of prefilters for discrete multiwavelet transforms," *IEEE Trans. Signal Proc.* **44**, pp. 25-35, 1996.
9. D. P. Hardin and D. W. Roach, "Multiwavelet prefilters I: Orthogonal prefilters preserving approximation order p<=2," *IEEE Trans. Circuits Syst. II* **45**, no. 8, pp. 1106-1112, 1998.
10. V. Strela and A. T. Walden, "Signal and image denoising via wavelet thresholding: Orthogonal and biorthogonal, scalar and multiple wavelet transforms," *Imperial College, Statistics Section*, Tech. Rep. TR-98-01, 1998.
11. J. S. Geronimo, D. P. Hardin, and P. R. Massopust, "Fractal functions and wavelet expansions based on several functions," *J. Approx. Theory* **78**, no. 3, pp. 373-401, 1994.
12. C. K. Chui and J. A. Lian, "A study of orthonormal multiwavelets," *Appl. Numer. Math.* **20**, pp. 273-298, 1995.
13. L.-X. Shen, H. H. Tan, and J. Y. Tham, "Symmetric-antisymmetric orthonormal multiwavelets and related scalar wavelets," *Applied and Computational Harmonic Analysis (ACHA)* **8**, no. 3, pp. 258-279, 2000.
14. A. Laine and J. Fan, "Texture classification by wavelet packet signatures," *IEEE Trans. Pattern Anal. Machine Intell.* **15**, no. 11, pp. 1186–1191, 1993.
15. M.-C. Lee and C.-M. Pun, "Texture classification using dominant wavelet packet energy features," in *Proc. IEEE Southwest Symposium*: *Image Analysis and Interpretation*, pp. 301–304, 2000.
16. Jain A, Dubes R., *Algorithms for clustering data*. New York: Prentice Hall Advanced Reference Series, 1988, pp. 130-142.